Abdominal Imaging

Published online: 25 June 2014

Abdom Imaging (2015) 40:120–126
DOI: 10.1007/s00261-014-0181-2

Zoomed echo-planar imaging using parallel transmission: impact on image quality of diffusion-weighted imaging of the prostate at 3T

Andrew B. Rosenkrantz,[1] Hersh Chandarana,[1] Josef Pfeuffer,[3] Michael J. Triolo,[1,4] Mohammed Bilal Shaikh,[1,5] David J. Mossa,[1] Christian Geppert[2]

[1]Department of Radiology, NYU Langone Medical Center, 550 First Avenue, New York, NY 10016, USA
[2]Siemens Medical Solutions MR R&D, 660 First Avenue, New York, NY 10016, USA
[3]Siemens Healthcare, Allee am Röthelheimpark 2, 91052 Erlangen, Germany
[4]Present address: Northport VA Medical Center, 79 Middleville Road, North Port, NY 11768, USA
[5]Present address: Winthrop-University Hospital, 259 1st St., Mineola, NY 11501, USA

Abstract

Purpose: To assess impact of two-channel parallel transmission (pTx) with focused excitation [zoomed echo-planar imaging (EPI)] on image quality of prostate diffusion-weighted imaging (DWI) at 3T.
Methods: 27 male volunteers (27 ± 8 years) underwent 3T prostate MRI using 2-channel radiofrequency-transmit system and 18-channel torso receive coil. Scans included EPI–DWI sequence (*b* values 50, 500, 1000 s/mm^2) acquired both with standard sinc pulse and 2-channel pTX with focused excitation, each acquired at large-field-of-view (FOV) (20 × 20 cm) and small-FOV (14 × 14 cm). An abdominal radiologist scored *b*-1000 images and ADC maps for image quality measures. Sequences were compared using paired Wilcoxon tests.
Results: pTx with focused excitation showed significant improvements compared with standard DWI on *b*-1000 images at large-FOV for the absence of wrap and overall image quality ($p \leq 0.049$); on *b*-1000 images at small-FOV for reduced distortion of prostate, absence of ghosting, absence of wrap, clarity of prostate capsule, clarity of peripheral/transition zone boundary, clarity of peri-urethral region, and overall image quality ($p \leq 0.004$); and on ADC maps at small-FOV for reduced distortion of prostate, sharpness of prostate, clarity of prostatic capsule, clarity of peri-urethral region, and overall image quality ($p = 0.002$–0.036). When compared with standard large-FOV images, small-FOV images obtained using pTx with focused excitation showed no significant difference on the *b*-1000 images for any feature ($p \geq 0.175$), while showing significant improvements on the ADC maps in terms of reduced distortion, absence of ghosting, and absence of wrap ($p = 0.010$–0.030).
Conclusion: Zoomed DWI using 2-channel pTx reduced artifacts and improved image quality for 3T prostate DWI; benefit was most apparent for small-FOV images.

Key words: Prostate cancer—MRI—Diffusion-weighted imaging—3T—Parallel transmission

Diffusion-weighted imaging (DWI) is a critical component of multi-parametric prostate MRI protocols, having established value in tumor detection and localization, guidance of risk assessment, and the performance of targeted biopsies [1–3]. However, given the use of an echo-planar imaging (EPI) technique, DWI of the prostate suffers from technical challenges relating to B_0- and B_1-field inhomogeneity and eddy currents that lead to anatomic distortion and image artifacts [4, 5]. Although recent guidelines support the routine performance of prostate MRI at 3T [6], these artifacts on DWI can be more problematic at 3T given increasing B_0 and B_1-inhomogeneity at the higher field strength [4, 5].

Correspondence to: Andrew B. Rosenkrantz; *email:* andrew.rosenkrantz@nyumc.org

Parallel transmission (pTx) is a recent technologic advance offering the potential to substantially improve upon these challenges [7–9]. Current implementations of pTx entail two-channel radiofrequency (RF) transmitter systems with the ability to independently adjust the phase and amplitude of each channel. This ability allows for patient- and volume-specific B_1-shimming, thereby achieving more homogeneous excitation within the field-of-view and a reduction of artifacts related to field-inhomogeneity. This approach has been previously studied in the upper abdomen at 3T and shown to significantly improve image quality and diagnostic accuracy for liver lesion detection on T2-weighted imaging (T2WI) [9, 10], as well as image quality for DWI [11]. However, some caution is warranted as the application of pTx for DWI in the upper abdomen did result in significant differences in apparent diffusion coefficient (ADC) value measurements, depending on the combination of *b* value and anatomic site [11].

An additional attribute of some 2-channel pTx systems, beyond just B_1-shimming, is the ability to perform 2-dimensional (2D) selective RF pulses that apply focused excitation of just an inner volume of tissue, thereby allowing for a substantial reduction of the FOV in the phase-encoding direction [12, 13]. This reduction in FOV and associated reduction in the number of phase-encoding steps can in turn provide a reduction in image distortion and other phase-encoding-related artifacts, as well as an increase in spatial resolution, thus improving image quality even further. To our knowledge, there has been only limited recent assessment of DWI with focused excitation using pTx systems in abstract form [14, 15].

Prostate cancer imaging would seem to be a natural application for a 2-channel pTx system offering both B_1 shimming and focused excitation. The artifacts and anatomic distortion frequently encountered in prostate DWI would be mitigated by the combination of B_1-shimming and reduced phase-encoding steps achieved by focused excitation, while the prostate's small size and deep position within the torso, as well as the small size of many prostate tumors, provide a good target for focused excitation. However, as the ADC values of prostate tumors are often clinically applied in a quantitative manner, the potential impact of pTx using focused excitation on ADC value reproducibility is of concern. Thus, the aim of this study was to evaluate the impact of 2-channel pTx using focused excitation on image quality of EPI DWI of the prostate at 3T.

Materials and methods

Subjects

This prospective study was HIPAA-compliant and approved by our institutional review board. 27 healthy male volunteers (mean age 27 ± 8, range 22–66) were recruited to undergo DWI of the prostate. All subjects provided written informed consent prior to the scan.

MRI technique

MRI was performed using a single 3T system (MAGNETOM Skyra, Siemens AG, Healthcare Sector) using a 2-channel pTx system, an 18-channel body matrix receive coil, and gradients with a peak amplitude of 45 mT/m and slew rate of 200 T/m/s. Following initial anatomic T2-weighted images obtained to localize the prostate, a series of axial single-shot (SS) double-refocused (bipolar) EPI DWI sequences of the prostate were performed. These DWI sequences were performed using tri-directional diffusion-sensitizing gradients with *b* values of 50, 500, and 1000 s/mm^2, performed with 4, 8, and 8 averages, respectively. Other parameters common to all DWI sequences included TR 6700 ms, slice thickness 3 mm, spectral adiabatic inversion recovery (SPAIR) for fat suppression, and parallel imaging using the GRAPPA technique and an acceleration factor within left–right phase-encoding direction of 2.

A total of four DWI sequences were obtained. First, two large-FOV acquisitions were performed, one using a standard sinc pulse and the other using 2-channel pTx with focused excitation; these were acquired with FOV 20 × 20 cm and matrix 90 × 90. Then, two small-FOV acquisitions, similar to the FOV generally used for endorectal-coil imaging of the prostate, were performed, again using both a standard sinc pulse and 2-channel pTx with focused excitation; these were acquired with FOV 14 × 14 cm and matrix 90 × 90. pTx was used to achieve B_1-shimming for all four acquisitions. These four sequences are hereafter referred to as large-FOV standard, large-FOV pTx, small-FOV standard, and small-FOV pTX, respectively. For all sequences, minimum TE was used (81 ms for standard EPI; 87 ms for pTx due to longer excitation pulse duration). Acquisition time was 7 min 56 s for small-FOV pTX and 7 min 16 s for the other sequences. For each of the four acquisitions, in-line calculation of the ADC map was performed using a mono-exponential fit based on the three obtained *b* values. Outer volume suppression was not applied in combination with any of the sequences.

Image analysis

A radiologist with fellowship training in abdominal imaging evaluated the *b*-1000 images and ADC maps from all acquisitions. Cases were evaluated in random order, and the observer was unaware as to whether images were obtained using standard transmission or pTx with focused excitation. The observer evaluated all *b*-1000 image sets and ADC maps in terms of anatomic distortion of the prostate relative to prostate shape on T2WI, clarity of the prostate capsule, clarity of the

boundary of the prostate peripheral and transition zones, clarity of the peri-urethral region, and overall image quality; and additionally evaluated *b*-1000 images for the absence of ghosting artifact and the absence of wrap artifact; and ADC maps for sharpness of the prostate peripheral zone. All categories were assessed on a 1–5 scale with 5 indicating the highest image quality; features relating to the presence of artifacts were scored as follows: 1 = marked artifact, non-diagnostic; 2 = marked artifact, moderately impacting diagnosis; 3 = moderate artifact, mildly impacting diagnosis; 4 = mild artifact, not impacting diagnosis; and 5 = excellent image quality.

A separate abdominal radiologist, also unaware of sequence details, placed a small region-of-interest (ROI) in a corresponding location of each lobe of the peripheral zone on both the *b*-1000 image set and the ADC map for each DWI acquisition for each case. The ROIs were placed on an area showing visually normal signal intensity (SI) and an absence of artifacts and had a mean size of 0.47 ± 0.19 cm^2 for large-FOV image sets and of 0.34 ± 0.09 cm^2 for small-FOV image sets. In similar fashion, a third abdominal radiologist placed a single ROI in the transition zone on the *b*-1000 image set and the ADC map for each DWI acquisition for each patient, having a mean size of 2.36 ± 0.72 cm^2 for large-FOV image sets and of 2.22 ± 0.49 cm^2 for small-FOV image sets. The mean and standard deviation (SD) of all ROIs were recorded. Given the presence of geometric variation in image noise across the image due to the use of parallel imaging for all sequences, as well as the lack of inclusion of background air in the small-FOV images, ROI measurements within air were not performed to represent image noise. Rather, the estimated signal-to-noise ratio (eSNR) corresponding to each ROI on the *b*-1000 images was calculated as the ratio between the mean and SD of the given ROI, consistent with a previous report regarding estimating SNR in the presence of parallel imaging [16]. The eSNR and ADC of both lobes of the peripheral zone were averaged to obtain a single peripheral zone value for each sequence.

Statistics

Subjective image quality scores were compared between combinations of sequences using paired Wilcoxon tests. Peripheral zone and transition zone eSNR and ADC measurements were compared between combinations of sequences using paired t tests. Analysis was performed using software (MedCalc version 10.4, Frank Schoonjans). All comparisons are two-sided and considered statistically significant at $p < 0.05$.

Results

Qualitative image quality

Representative cases are shown in Figs. 1 and 2. Tables 1 and 2 show the results of the subjective assessments of the *b*-1000 images and ADC maps from the four DWI sequences for the two observers. For the *b*-1000 image sets, large-FOV pTx showed significant improvements in comparison with large-FOV standard in terms of the absence of wrap artifact and overall image quality ($p \leq 0.049$), but no significant difference in terms of other assessed features ($p \geq 0.080$), while small-FOV pTx showed highly significant improvements in comparison

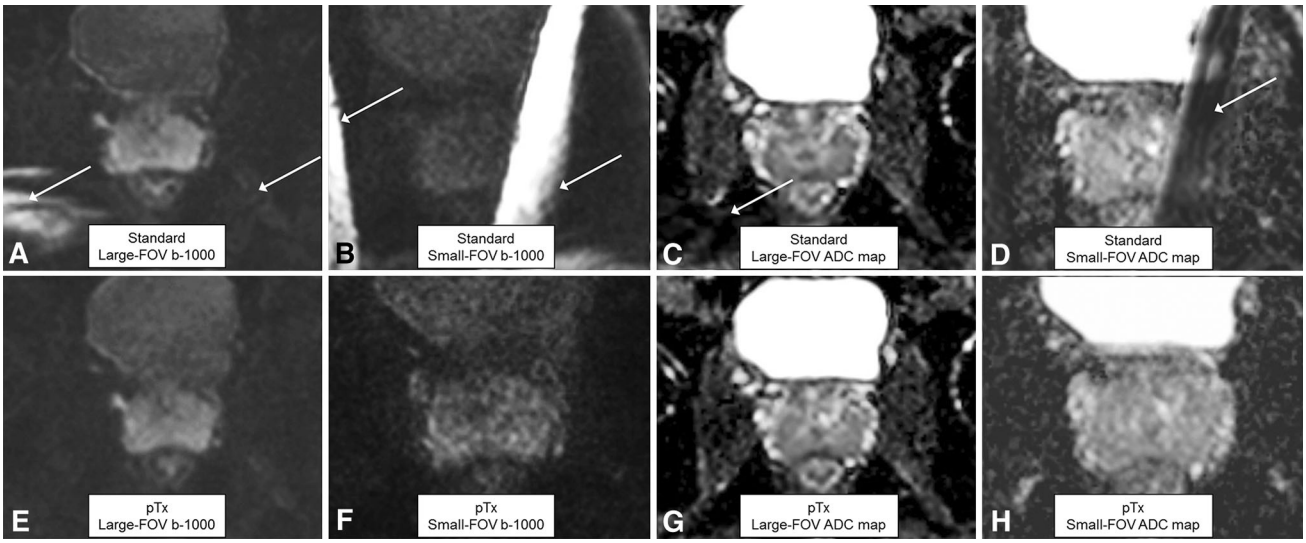

Fig. 1. 26-year-old healthy male volunteer undergoing DWI of the prostate. Standard large-FOV *b*-1000 image, small-FOV *b*-1000, large-FOV ADC map, and small-FOV ADC map (**A**, **B**, **C**, and **D**, respectively), as well as parallel transmission with focused excitation (pTx) large-FOV *b*-1000 image, small-FOV *b*-1000, large-FOV ADC map, and small-FOV ADC map (**E**, **F**, **G**, and **H**, respectively), are shown. Numerous artifacts on standard images (*arrows*) are substantially improved on pTx images.

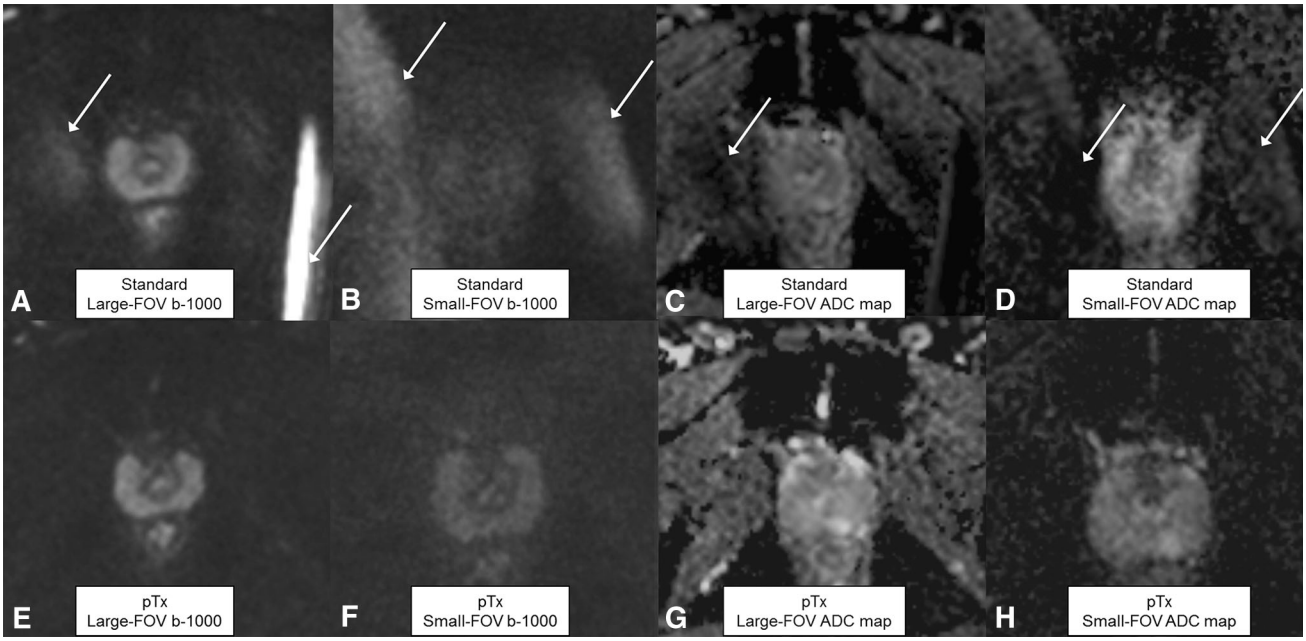

Fig. 2. 27-year-old healthy male volunteer undergoing DWI of the prostate. Standard large-FOV *b*-1000 image, small-FOV *b*-1000, large-FOV ADC map, and small-FOV ADC map (**A**, **B**, **C**, and **D**, respectively), as well as parallel transmission with focused excitation (pTx) large-FOV *b*-1000 image, small-FOV *b*-1000, large-FOV ADC map, and small-FOV ADC map (**E**, **F**, **G**, and **H**, respectively), are shown. Numerous artifacts on standard images (*arrows*) are substantially improved on pTx images.

Table 1. Comparison of subjective image quality scores (mean ± SD) between *b*-1000 images obtained using different diffusion-weighted imaging sequences of the prostate

Feature	Large-FOV standard	Large-FOV pTx*	*p***	Small-FOV standard	Small-FOV pTx*	*p***
Reduced distortion of prostate	4.0 ± 0.9	4.3 ± 0.9	0.110	3.0 ± 1.1	3.9 ± 0.9	**0.004**
Absence of ghosting artifact	4.0 ± 0.9	4.3 ± 0.7	0.080	2.7 ± 1.0	3.9 ± 1.0	**<0.001**
Absence of wrap artifact	3.4 ± 1.0	4.2 ± 0.8	**0.001**	2.0 ± 0.9	3.6 ± 1.1	**<0.001**
Clarity of capsule	4.3 ± 0.7	4.3 ± 0.8	0.820	3.0 ± 1.3	4.0 ± 0.9	**<0.001**
Clarity of peripheral/transition zone boundary	4.1 ± 0.9	4.4 ± 0.9	0.244	3.0 ± 1.2	4.1 ± 0.9	**<0.001**
Clarity of peri-urethral region	4.4 ± 0.9	4.6 ± 0.7	0.375	3.0 ± 1.3	4.1 ± 0.8	**<0.001**
Overall image quality	4.0 ± 0.9	4.4 ± 0.9	**0.049**	2.6 ± 0.9	4.0 ± 0.9	**<0.001**

* Refers to combination of 2-channel pTx system incorporating B_1-shimming and focused excitation
** Listed in bold when statistically significant at $p < 0.05$

with small-FOV standard in terms of all assessed features (reduced distortion of prostate, the absence of ghosting artifact, the absence of wrap artifact, clarity of capsule, clarity of peripheral/transition zone boundary, clarity of peri-urethral region, and overall image quality; $p \leq 0.004$). For the ADC maps, there was no significant difference between large-FOV pTx and large-FOV standard for any comparison ($p \geq 0.098$), although small-FOV pTx showed significant improvements in comparison with small-FOV standard in terms of reduced distortion of the prostate, sharpness of prostate, clarity of prostatic capsule, clarity of peri-urethral region, and overall image quality ($p = 0.002$–0.036); there was no significant difference in terms of clarity of peripheral/transition zone boundary ($p = 0.294$).

Additional comparisons were performed between large-FOV and small-FOV images. For *b*-1000 images, large-FOV standard received significantly better scores than small-FOV standard for all features ($p \leq 0.004$). However, large-FOV standard and small-FOV pTx showed no significant difference for any feature ($p \geq 0.175$). In addition, large-FOV pTx received significantly better scores than small-FOV pTx in terms of reduced distortion, absence of ghosting artifact, and absence of wrap artifact ($p = 0.010$–0.030), while the other features were not significantly different ($p \geq 0.074$).

For the ADC map, large-FOV standard and small-FOV standard showed no significant difference for any feature ($p \geq 0.170$); large-FOV pTx and small-FOV pTx also showed no significant difference for any feature ($p \geq 0.080$). However, small-FOV pTx received significantly better scores than large-FOV standard in terms of reduced distortion, sharpness of the prostate, and overall image quality ($p = 0.023$–0048).

Table 2. Comparison of subjective image quality scores (mean ± SD) between ADC maps obtained using different diffusion-weighted imaging sequences of the prostate

Feature	Large-FOV standard	Large-FOV pTx*	*p*	Small-FOV standard	Small-FOV pTx*	*p***
Reduced distortion of prostate	3.4 ± 0.9	3.8 ± 0.8	0.098	3.0 ± 1.1	4.0 ± 1.0	**0.002**
Sharpness of prostate	3.1 ± 0.7	3.2 ± 0.8	0.579	2.8 ± 1.0	3.6 ± 1.0	**0.004**
Clarity of capsule	3.2 ± 0.8	3.5 ± 0.7	0.173	3.0 ± 1.0	3.5 ± 1.0	**0.015**
Clarity of peripheral/transition zone boundary	3.0 ± 1.0	2.8 ± 0.8	0.421	2.9 ± 1.1	3.1 ± 1.0	0.294
Clarity of peri-urethral region	2.9 ± 0.9	2.9 ± 0.7	0.890	2.7 ± 1.0	3.3 ± 1.1	**0.036**
Overall image quality	3.1 ± 0.8	3.3 ± 0.7	0.433	2.9 ± 1.0	3.6 ± 1.0	**0.005**

* Refers to combination of 2-channel pTx system incorporating B_1-shimming and focused excitation
** Listed in bold when statistically significant at $p < 0.0$

Table 3. Comparison of eSNR and ADC values, listed as mean ± SD, between DWI sequences of the prostate

Feature	Large-FOV standard	Large-FOV pTx*	*p*	Small-FOV standard	Small-FOV pTx*	*p***
Peripheral zone						
eSNR	26.2 ± 14.2	30.8 ± 18.3	0.126	16.7 ± 13.9	15.3 ± 6.1	0.700
ADC***	1.25 ± 0.22	1.24 ± 0.21	0.610	1.22 ± 0.22	1.17 ± 0.21	**<0.001**
Transition zone						
eSNR	8.9 ± 1.8	8.5 ± 1.6	0.256	7.5 ± 2.4	7.3 ± 2.9	0.339
ADC***	1.24 ± 0.11	1.23 ± 0.11	0.231	1.08 ± 0.16	1.07 ± 0.16	0.256

* Refers to combination of 2-channel pTx system incorporating B_1-shimming and focused excitation
** Listed in bold when statistically significant at $p < 0.05$
*** $\times 10^{-3}$ mm^2/s

Quantitative assessments

Table 3 shows the results of the quantitative assessments of the four DWI sequences. In both the peripheral and transition zones, eSNR at small-FOV, whether using standard or pTx, was consistently lower than eSNR at large-FOV, whether using standard or pTx ($p \leq 0.030$), aside from the comparison of eSNR in the transition zone between large-FOV pTx and small-FOV standard ($p = 0.070$). However, in both zones, there was no significant difference in eSNR between standard and pTx acquisitions at either the large- or small-FOV ($p \geq 0.126$). In the peripheral zone, ADC for small-FOV pTx was significantly less than for the other three acquisitions ($p < 0.001$), while there was no significant difference in ADC for any other comparison of sequences ($p \geq 0.081$). In the transition zone, ADC using small-FOV sequence was significantly lower than that using large-FOV sequence ($p < 0.001$), while there was no significant difference in ADC between the sequences at a constant FOV ($p = 0.231$–0.256).

Discussion

In this study, we provide to our knowledge the first report within the peer-reviewed literature of the impact of 2-channel pTx combining B_1-shimming and focused excitation on image quality of DWI of the prostate at 3T, and one of the first assessments of this technology in any anatomic region [14, 15]. Through independent adjustment of the phase and amplitude of two separate RF channels, pTx is able to perform patient- and volume-specific B_1-shimming and achieve greater B_1 homogeneity. However, an additional benefit of pTx on some systems is the ability to apply more complex excitation schemes that selectively excite a targeted inner volume of tissue, not only allowing for reduced FOV-imaging but also allowing for a reduction in phase-encoding steps and subsequent reduction in image distortions. While outer volume suppression may also be used to attempt selective tissue imaging [17], it is more difficult to achieve robust inner volume imaging using this approach in comparison with focused excitation, which is easily and reliably performed using the 2-channel pTx system evaluated in our study.

We evaluated pTx with focused excitation both at a large-FOV as well as at a small-FOV, comprising limited coverage tightly focused on the prostate. Our data demonstrate that 2-channel pTx combining B_1-shimming and focused excitation led to improvements in several measures relating to artifacts, anatomic distortion, and anatomic clarity compared to DWI of the prostate performed using a standard sinc pulse. The benefits of pTx with focused excitation were overall more pronounced for the high *b* value images than for the ADC maps. This may relate to some artifacts, such as wrap and ghosting artifact, being visually more apparent on the high *b* value images. Our findings are similar to the results of a previously published report of pTx for DWI that showed improved homogeneity and image quality on high *b* value images in the upper abdomen [11]. Improved image quality of the high *b* value images is important given that current expert panel guidelines for prostate MRI

interpretation incorporate findings on both the high *b* value images and the ADC map in stratifying the level of suspicion for tumor using DWI [6].

The benefit of pTx with focused excitation compared with standard excitation was even more pronounced for small-FOV images than for the comparison at a large-FOV. Indeed, all of the assessed image quality factors relating to distortion, artifacts, and anatomic clarity were significantly improved using focused excitation at small-FOV for the high *b* values images. In addition, a number of cases in which small-FOV images obtained using standard excitation were essentially non-diagnostic demonstrated substantially improved image quality using pTx with focused excitation. These more striking comparisons of the small-FOV images provide a compelling demonstration of the potential value of those pTx systems that provide not just improved B_1 homogeneity but are also capable of focused excitation. For the *b*-1000 images, while small-FOV standard was significantly worse than large-FOV standard in terms of all subjective measures, there was no significant difference in subjective quality between small-FOV pTx and large-FOV standard; furthermore, for the ADC maps, small-FOV pTx performed significantly better than large-FOV standard in terms of several image quality measures. Therefore, when considering image quality of the *b*-1000 images and the ADC map, as well as spatial resolution, small-FOV pTx imaging offers an intriguing possibility for prostate DWI. To this end, future studies are warranted to assess whether small-FOV DWI of the prostate using pTx with focused excitation may enable clinical prostate DWI using a reduced FOV that is similar to the FOV of endorectal-coil imaging, while using solely a pelvic phased-array coil.

An interesting finding was the small but significant decrease in ADC of peripheral zone using pTx with focused excitation at the small-FOV, and of transition zone for both small-FOV sequences. Past work has suggested that lowering of SNR of DWI to a noise floor can yield underestimation of ADC values [18, 19], which may partly account for the findings given consistently reduced eSNR at small-FOV. Furthermore, both the fewer number of phase-encoding steps and the moderate lengthening of TE of the spatially selective pTx sequence evaluated in our study are associated with reduction in SNR. However, the compared sequences at each FOV did not show a significant difference in eSNR in either zone. In addition, we note that Guo et al. [11] reported lower ADC in the spleen using pTx in the absence of an observed reduction in SNR, although were unable to establish an etiology for the difference. Likewise, the precise cause for the small but statistically significant reduction in peripheral zone ADC that we observed at small-FOV using pTx with focused excitation in comparison with standard excitation remains unknown from our data set. Nonetheless, given the quantitative manner in which ADC values of prostate tumors are applied in clinical practice [20, 21], these observations merit further investigation, and caution is advised if serial prostate MRI examinations in a given patient are performed using variable FOV or variable application of pTx with focused excitation between examinations.

The primary limitation of this study is that only healthy volunteers were evaluated. Thus, the impact of pTx with focused excitation on diagnostic performance using DWI in a patient setting, as well as on ADC values of tumors, still requires further study. In addition, imaging was performed without an endorectal coil, such that the behavior of DWI using pTx with focused excitation in the context of endorectal-coil imaging is unknown. However, as a potential motivation for pTx with focused excitation in prostate imaging is to obtain high-quality small-FOV (approximately 140 mm) images without use of an endorectal coil, assessment using a pelvic phased-array coil, as was performed in this study, seems appropriate. Also, inter-reader reproducibility was not assessed. An additional limitation is that image quality was evaluated for a single *b* value. However, the high *b* value of the images assessed in this study is a maximal *b* value often used in clinical prostate imaging. Also, the considerably greater values for eSNR observed in the peripheral zone than in the transition zone are unexpected. This finding may relate to the substantially larger ROIs used in the transition zone, leading to wider SDs and subsequent reduced eSNR values computed using the applied eSNR formula. Nonetheless, consistent trends were observed in the two zones when comparing eSNR between small-FOV and large-FOV images or between standard and pTx. Finally, given the exploratory nature of our study investigating a new technique, we did not apply statistical corrections for multiple comparisons, in order to avoid substantially reducing our ability to detect potentially clinically important differences meriting further, more definitive, evaluation.

Conclusion

We demonstrated improved image quality for prostate DWI at 3T using pTx with focused excitation. The benefit in image quality was most apparent for small-FOV high *b* value images, raising the possibility of using this acquisition approach clinically for high-quality small-FOV images without an endorectal coil. Thus, additional studies assessing the impact of pTx with focused excitation on prostate cancer detection in a clinical setting remain warranted.

Acknowledgment. Two authors (CG and JP) are employees of Siemens; however, neither Siemens nor these authors provided any funding for the project and the remaining authors had control over all data.

References

1. Haider MA, van der Kwast TH, Tanguay J, et al. (2007) Combined T2-weighted and diffusion-weighted MRI for localization of prostate cancer. AJR Am J Roentgenol 189(2):323–328
2. Somford DM, Hambrock T, Hulsbergen-van de Kaa CA, et al. (2012) Initial experience with identifying high-grade prostate cancer using diffusion-weighted MR imaging (DWI) in patients with a Gleason score </= 3 + 3 = 6 upon schematic TRUS-guided biopsy: a radical prostatectomy correlated series. Invest Radiol 47(3):153–158
3. Hambrock T, Hoeks C, Hulsbergen-van de Kaa C, et al. (2012) Prospective assessment of prostate cancer aggressiveness using 3-T diffusion-weighted magnetic resonance imaging-guided biopsies versus a systematic 10-core transrectal ultrasound prostate biopsy cohort. Eur Urol 61(1):177–184
4. Akisik FM, Sandrasegaran K, Aisen AM, Lin C, Lall C (2007) Abdominal MR imaging at 3.0 T. Radiographics 27(5):1433–1444
5. Lee VS, Hecht EM, Taouli B, et al. (2007) Body and cardiovascular MR imaging at 3.0 T. Radiology 244(3):692–705
6. Barentsz JO, Richenberg J, Clements R, et al. (2012) ESUR prostate MR guidelines 2012. Eur Radiol 22(4):746–757
7. Nelles M, Konig RS, Gieseke J, et al. (2010) Dual-source parallel RF transmission for clinical MR imaging of the spine at 3.0 T: intraindividual comparison with conventional single-source transmission. Radiology 257(3):743–753
8. Murtz P, Kaschner M, Traber F, et al. (2012) Evaluation of dual-source parallel RF excitation for diffusion-weighted whole-body MR imaging with background body signal suppression at 3.0 T. Eur J Radiol 81(11):3614–3623
9. Willinek WA, Gieseke J, Kukuk GM, et al. (2010) Dual-source parallel radiofrequency excitation body MR imaging compared with standard MR imaging at 3.0 T: initial clinical experience. Radiology 256(3):966–975
10. Kukuk GM, Gieseke J, Weber S, et al. (2011) Focal liver lesions at 3.0 T: lesion detectability and image quality with T2-weighted imaging by using conventional and dual-source parallel radiofrequency transmission. Radiology 259(2):421–428
11. Guo L, Liu C, Chen W, Chan Q, Wang G (2013) Dual-source parallel RF transmission for diffusion-weighted imaging of the abdomen using different b values: Image quality and apparent diffusion coefficient comparison with conventional single-source transmission. J Magn Reson Imaging 37(4):875–885
12. Schneider R, Ritter D, Haueisen J, Pfeuffer J (2012) Novel 2DRF optimization framework for spatially selective rf pulses incorporating B1, B0 and variable density trajectory. In: Proceedings of the 20th scientific meeting, International Society for Magnetic Resonance and Medicine, Melbourne, p 1884
13. Schneider R, Ritter D, Haueisen J, Pfeuffer J (2012) Evaluation of 2DRF echo-planar pulse designs for parallel transmission. In: Proceedings of the 20th scientific meeting, International Society for Magnetic Resonance and Medicine, Melbourne, p 1928
14. Geppert C, Glielmi C, Brown R, et al. (2013) Application of zoomed EPI and pTX for breast diffusion weighted imaging. In: Proceedings of the 21st scientific meeting, Internatinoal Society for Magnetic Resoance in Medicine, Salt Lake City, UT, p 1739
15. Futterer J, Chandarana H, Rusinek H, et al. (2013) Feasibility of kidney DTI using parallel transmission in normal volunteers. In: Proceedings of the 21st scientific meeting, International Society for Magnetic Resonance in Medicine, Salt Lake City, UT, p 1554
16. Heverhagen JT (2007) Noise measurement and estimation in MR imaging experiments. Radiology 245(3):638–639
17. Tang L, Wen Y, Zhou Z, et al. (2013) Reduced field-of-view DTI segmentation of cervical spine tissue. Magn Reson Imaging 31(9):1507–1514
18. Bulow R, Mensel B, Meffert P, et al. (2012) Diffusion-weighted magnetic resonance imaging for staging liver fibrosis is less reliable in the presence of fat and iron. Eur Radiol 23:1281–1287
19. Dale BM, Braithwaite AC, Boll DT, Merkle EM (2010) Field strength and diffusion encoding technique affect the apparent diffusion coefficient measurements in diffusion-weighted imaging of the abdomen. Invest Radiol 45(2):104–108
20. Giles SL, Morgan VA, Riches SF, et al. (2011) Apparent diffusion coefficient as a predictive biomarker of prostate cancer progression: value of fast and slow diffusion components. AJR Am J Roentgenol 196(3):586–591
21. Park SY, Kim CK, Park BK, Lee HM, Lee KS (2011) Prediction of biochemical recurrence following radical prostatectomy in men with prostate cancer by diffusion-weighted magnetic resonance imaging: initial results. Eur Radiol 21(5):1111–1118